Bull Volcanol (2013) 75:708
DOI 10.1007/s00445-013-0708-3

RESEARCH ARTICLE

The 1815 Tambora ash fall: implications for transport and deposition of distal ash on land and in the deep sea

Jessica Kandlbauer · Steven N. Carey · R. Stephen J. Sparks

Received: 11 September 2012 / Accepted: 4 March 2013 / Published online: 23 March 2013

Abstract Tambora volcano lies on the Sanggar Peninsula of Sumbawa Island in the Indonesian archipelago. During the great 1815 explosive eruption, the majority of the erupted pyroclastic material was dispersed and subsequently deposited into the Indian Ocean and Java Sea. This study focuses on the grain size distribution of distal 1815 Tambora ash deposited in the deep sea compared to ash fallen on land. Grain size distribution is an important factor in assessing potential risks to aviation and human health, and provides additional information about the ash transport mechanisms within volcanic umbrella clouds. Grain size analysis was performed using high precision laser diffraction for a particle range of 0.2 μm–2 mm diameter. The results indicate that the deep-sea samples provide a smooth transition to the land samples in terms of grain size distributions despite the different depositional environments. Even the very fine ash fraction (<10 μm) is deposited in the deep sea, suggesting vertical density currents as a fast and effective means of transport to the seafloor. The measured grain size distribution is consistent with an improved atmospheric gravity current sedimentation model that takes into account the finite duration of an eruption. In this model, the eruption time and particle fall velocity are the critical parameters for assessing the ash component depositing while the cloud advances versus the ash component depositing once the eruption terminates. With the historical data on eruption duration (maximum 24 h) and volumetric flow rate of the umbrella cloud (~$1.5–2.5\times10^{11}$ m^3/s) as input to the improved model, and assuming a combination of 3 h Plinian phase and 21 h co-ignimbrite phase, it reduces the mean deviation of the predicted versus observed grain size distribution by more than half (~9.4 % to ~3.7 %) if both ash components are considered.

Keywords Tephra fall deposits · Tephra dispersion · Deep sea sedimentation · Explosive eruption · Tambora

Editorial responsibility: S. A. Fagents

J. Kandlbauer (✉) · R. S. J. Sparks
Department of Earth Sciences, University of Bristol,
Wills Memorial Building, Queen's Road,
BS8 1RJ, Bristol, UK
e-mail: J.Kandlbauer@bristol.ac.uk

S. N. Carey
Graduate School of Oceanography, University of Rhode Island,
South Ferry Road,
Narragansett, RI 02882, USA

Introduction

The 1815 Tambora eruption was one of the largest magnitude explosive eruptions in the last 1,000 years with a minimum volume of 30 km^3 DRE (Self et al. 2004). An initial Plinian eruption occurred on 5 April (estimated column height 33 km; Sigurdsson and Carey 1989) after 3 years of minor activity (e.g. Ross 1816; Stewart 1820; Crawfurd 1856; Zollinger 1855; Stothers 1984; Sigurdsson and Carey 1989). The climactic phase of the eruption started on the evening of 10 April, with a major Plinian eruption (estimated column height 43 km; Sigurdsson and Carey 1989) and pyroclastic flow formation (e.g. Ross 1816; Raffles 1817; Stothers 1984). The umbrella cloud covered an area of at least 980,000 km^2 during the climactic phase, and the sky did not clear for 3 days in the Jakarta area, 1,300 km from the volcano (Ross 1816; Self et al. 2004). Ash fall was reported as far as 1,800 km to the west of Tambora (Crawfurd 1856).

Studying distal fine ash of an eruption that occurred almost 200 years ago raises some difficulties since fine ash in distal areas is typically reworked and redeposited quickly by precipitation, wind and human activities on land (Rose and Durant 2009). In addition, Tambora is situated on the Indonesian island of Sumbawa and surrounded by the sea

(Fig. 1); thus, ash was deposited both on land and on the sea floor.

Ash deposits in deep-sea cores have been studied primarily to refine the chronology of volcanic eruptions using geochemical data and lithology, as well as to improve ash dispersal maps, thickness estimates and eruption dynamics (e.g. Watkins et al. 1978; Rose and Chesner 1987; Sigurdsson et al. 1980). However, analysing the physical attributes, such as grain size distribution of distal volcanic ash, is important for assessing ash hazard to the environment, notably in the context of human health (Horwell 2007) and aviation safety (Casadevall 1994).

Comparing the grain size distribution of land and deep-sea samples will help to understand whether the different depositional environments affect the ash deposition, and consequently allow for the assessment of ash transport mechanisms in the volcanic umbrella cloud leading to the observed grain size distribution. Ash fall distributions and grain size characteristics can be compared with theoretical models of ash transport and deposition in umbrella clouds (e.g. Sparks et al. 1991; Bursik et al. 1992; Baines and Sparks 2005).

Samples and methods

Grain size analysis of the distal 1815 Tambora ash has been performed on four deep-sea ash layers and five land samples (Fig. 1 and Table 1). The deep-sea samples have been collected from the Snellius 2 expedition cores (1984), stored at NIOZ (Royal Netherlands Institute for Sea Research, Texel), and complemented with samples already collected by C. Mandeville at GSO/URI (Graduate School of Oceanography, University of Rhode Island). The ash layers were sampled approximately every 2 cm vertically throughout the cores if possible. Previous studies of more proximal cores (Saleh Bay and adjacent sea; Fig. 1) revealed only very little volcanic material (Zen and Ganie 1992).

Distal ash land samples used for this study were obtained during fieldwork in the Tambora area by Sigurdsson and Carey (1989). All fine ash smaller than 2 mm has been collected at each location. Although previously identified as co-ignimbrite ash (F5 layer; Sigurdsson and Carey 1989), there are no clear characteristics that could distinguish the co-ignimbrite ash from the fine Plinian ash. Thus, land samples could contain a mixture of both.

Grain size analysis

All deep-sea samples were treated with acetic acid to remove the carbonate fraction, and the land samples were cleaned to remove organic matter (e.g. small roots). Deep-sea samples containing a substantial amount of silicic biogenic particles were not considered for grain size analysis. Before the grain size analysis, a sodium hexametaphosphate solution (5 ml) was used to deflocculate clay particles, and samples were put in a sonic bath for 10 min to disperse possible sediment aggregates.

Grain size analysis was performed using a laser diffractometer Malvern Mastersizer 2000, which is able to measure the distribution of ash as fine as 0.02 μm and up to 2 mm. The Mastersizer acquires the light scattering pattern of the particles according to the Fraunhofer theory (used for this study). The Mastersizer assumes an equivalent spherical particle diameter. Most ash particles in the Tambora deposit have low aspect ratios, and shapes do not differ much among grain sizes. Thus, an equivalent spherical diameter is a reasonable approximation, and size-dependent effects on the results are not expected. The Mastersizer 2000 is very susceptible to clogging by large particles, and all land samples were consequently passed through a 500-μm sieve. The volume proportions of >500 μm particles accounted for less than 1 %.

Results

Depositional characteristics of distal marine ash deposits

The lower intervals of the ash layer (24–26 and 22–24 cm) in core G6.5 show a distinct bimodal grain size distribution, while the successive upper intervals gradually turn into unimodal and finer-grained ash (Fig. 2a). The coarse mode occurs at 400 μm, while the fine mode has its maximum at 20 μm in the sample at 24–26 cm. With decreasing depth, the two maxima progressively converge to a constant fine mode at the expense of the coarse mode. The mode of the unimodal samples in the upper intervals 14–16, 12–14, 10–12, 6–8 and 4–6 cm decreases from 75 to 35 μm. A similar pattern is observed in deep-sea core T84-37 (Fig. 2b), with clear bimodal and coarser-grained ash in sample intervals 24–26, 22–24 and 20–22 cm. Unlike core G6.5, the bimodal and coarser grained ash in core T84-37 is underlain by two unimodal and finer grained layers (26–28 and 28–30 cm) with modes at 45 and 35 μm, respectively. The overlying bimodal intervals (20–22, 22–24 and 24–26 cm) have a coarser mode around 100–150 μm and a finer mode around 25 μm. The upper unimodal intervals (16–18 and 12–14 cm) have modes at 40 and 25 μm, respectively. The ash layers in T84-42 and T84-27 show unimodal distributions with grain size maxima at 30 and 40 μm, respectively (Fig. 2c). T84-27 shows a minor peak below 10 μm possibly indicating a small amount of background material (some silicic biogenic particles were detected). However, the mode is still representative of the ash fall deposit.

Depositional characteristics of distal ash deposit on land

The particle sizes of the land deposits decrease with increasing distance from the vent. The samples up to 65 km [TB-

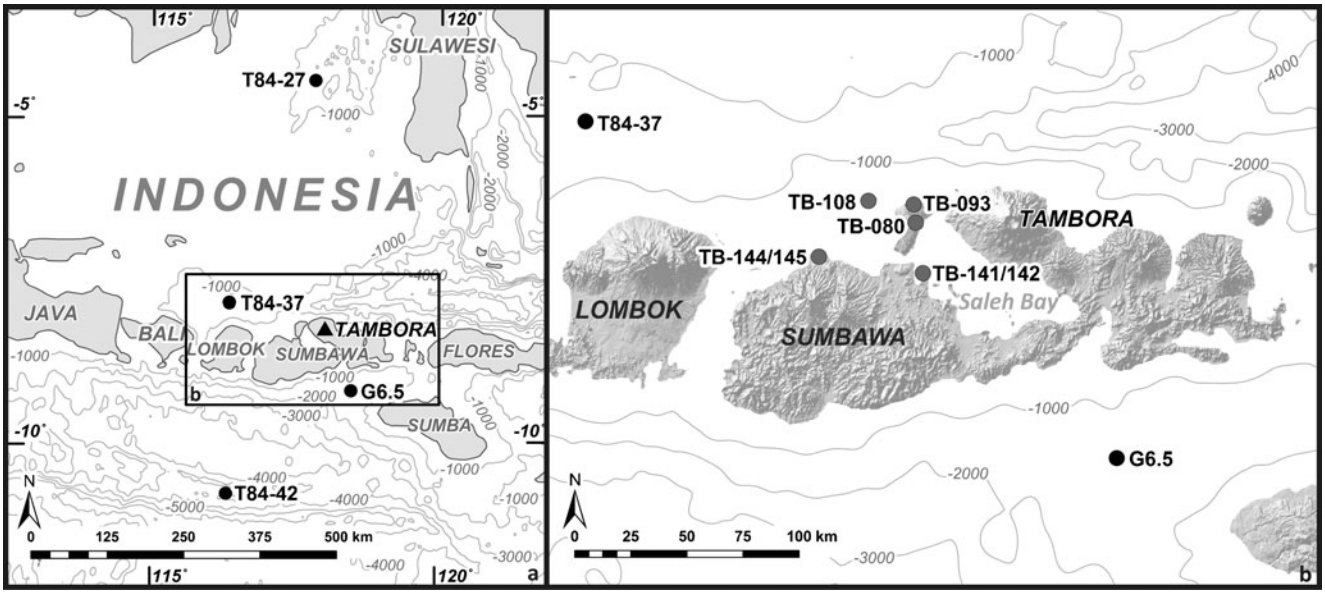

Fig. 1 Map showing the location of Tambora volcano and the studied samples from the deep sea (*black circles*) and on land (*grey circles*). Map source: ESRI (2009); bathymetry source: Amante and Eakins (2009)

141/142 (43 km), TB-080 (44 km), TB-093 (47 km) and TB-108 (65 km)] all show a mode at around 200 μm, with a minor secondary mode around 20–30 μm (Fig. 3). Sample TB-144/145 at 93 km distance is of unimodal nature with a mode at around 70/80 μm. All land samples have coarser modes than the more distal marine samples.

Distal grain size distribution in the deep sea and on land

The land and deep-sea samples together cover a distance from 43 to 422 km from Tambora, and grain size ranges from 1 μm up to 1 mm. All samples are poorly to very poorly sorted with sorting coefficients ranging from 1.77 to 2.34 ϕ. The spatial coverage is mostly to the west and southwest for the land samples, while deep-sea samples are distributed in all directions. Tambora ash has been found and analysed for the first time towards the south (T84-42) and southeast (G6.5).

The grain size cumulative averages for land and sea samples with distance are shown in Fig. 4. Grain size decreases with distance (Fig. 4a), and there is a smooth transition in grain size distribution with the progression from land to deep-sea samples (Fig. 4b). The proportion of coarse component (>125 μm) decreases substantially from 51 % of the relative size distribution at 43 km to 2 % at 422 km distance (Fig. 4b).

To assess the extent to which the very fine ash has been deposited and preserved on land and in the deep sea cores, the volumetric proportions of the 4- and 2.5-μm fractions, and the

Table 1 Description of land and deep-sea samples

Sample	Environment	Distance (km)	Location	Thickness (cm)	Intervals
TB141/142	Land	43	−8.42°, 117.67°	20.5	141: lower F4 layer 142: upper F5 layer
TB-080	Land	44	−8.19°, 117.67°	11	
TB-093	Land	47	−8.15°, 117.58°	15	
TB-108	Land	65	−8.13°, 117.42°	13	
TB-144/145	Land	93	−8.37°, 117. 16°	20	144: upper F5 layer 145: lower F layer
G6.5	Deep sea (depth, 2,070 m)	120	−9.21°, 118.46°	20	4–6, 6–8, 8–10, 10–12, 12–14, 14–16, 16–18, 18–20, 20–22, 22–24 and 24–26 cm
T84-37	Deep sea (depth, 1,530 m)	190	−7.86°, 116.33°	20	12–14, 16–18, 20–22, 22–24, 24–26, 26–28 and 28–30 cm
T84-42	Deep sea (depth, 3,150 m)	340	−10.78°, 116.3°	4	2.5–3 and 3–5 cm
T84-27	Deep sea (depth, 1,990 m)	422	−4.46°, 117.8°	3	11–13 cm

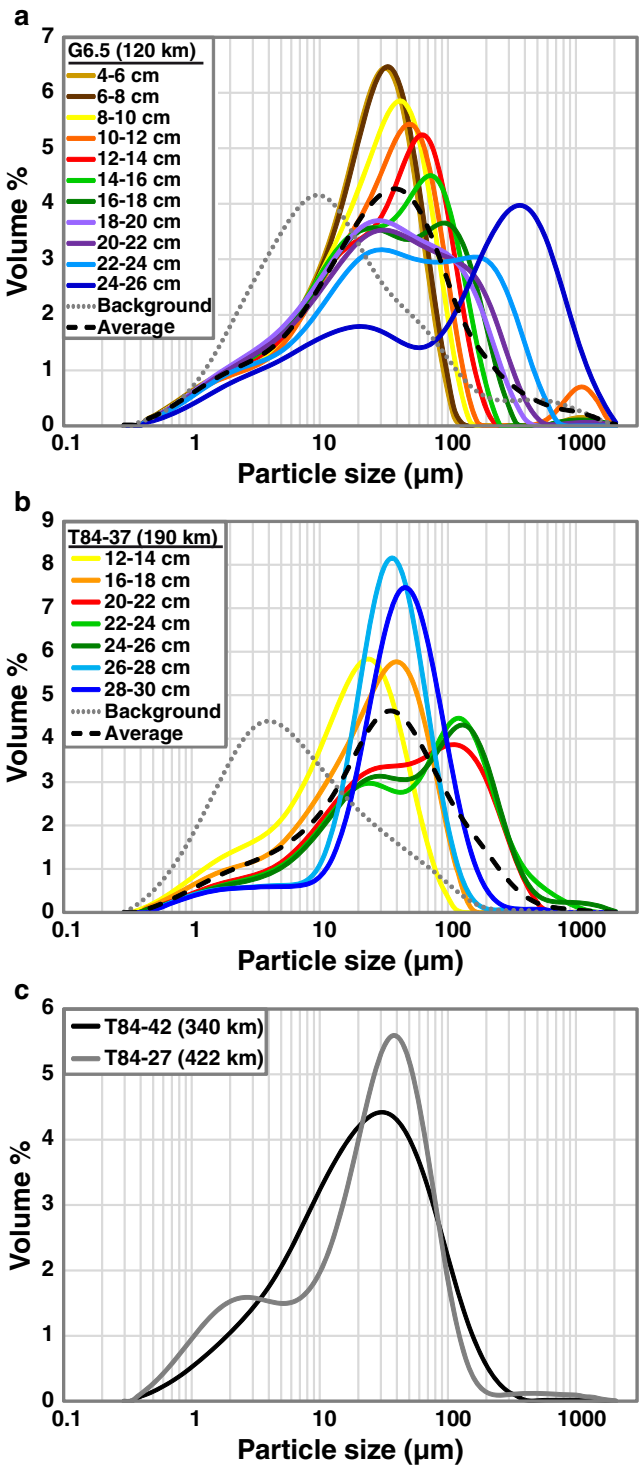

Fig. 2 Grain size distribution of deep-sea cores (**a**) G6.5, (**b**) T84-37, (**c**) T84-42 and T84-27. The legends in (**a**) and (**b**) refer to the depth of the sampling intervals in each deep-sea core. Note the transition from a bimodal distribution with a dominant coarse-ash mode at the bottom of the section to a fine-ash unimodal distribution at the top of cores G6.5 and T84-37. The two fine-grained unimodal layers at the base of T84-37 likely represent the first Plinian eruption from 5 April 1815

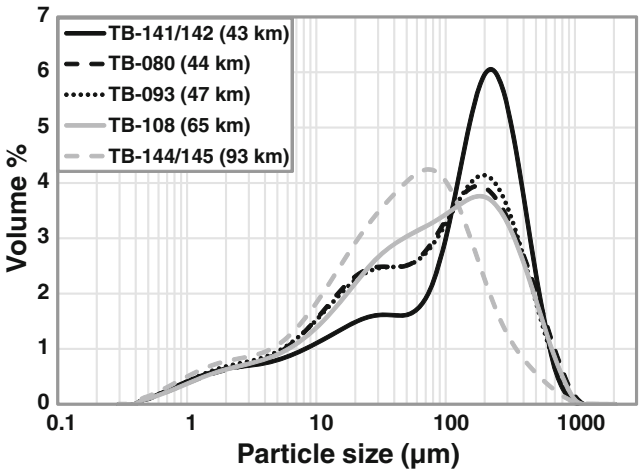

Fig. 3 Grain size distributions of land samples. Note the decreasing mode with increasing distance. Samples up to 65 km have a maximum at around 200 μm and minor secondary mode around 20–30 μm

10- and 4-μm fractions were considered and compared with the results of Horwell (2007). Horwell (2007) identified a strong correlation among the volumetric proportions of these size fractions in 63 samples of volcanic ash from eruptions of different style and distance from source (grey circles; Fig. 5a, b). The volumetric proportions of the Tambora ash (black and white circles; Fig. 5a, b) show only minor deviations from this correlation, independent of the depositional environment.

Discussion

Comparison of land and deep-sea deposits and transportation in the deep sea

The observation that grain size distribution in the deep-sea core deposits provides a continuum from the land samples (Fig. 4), and that even the very fine grain size fractions (<10 μm) are present with the same volumetric proportions as on land (Fig. 5), suggests that the ash deposited in the deep sea has not been significantly affected by the marine environment and is therefore comparable to the land deposits in terms of grain size distribution.

The abundance of fine ash in the deep-sea deposits implies a fast and effective way of transportation through the water column. Carey (1997) calculated, following the experiments of Fisher (1965), that particles of <15 μm will take more than 6 months to pass through a water column of 2,000 m by passive settling (Stokes law). Thus, significant redistribution of the fine ash particles by ocean currents would be expected. Aggregation of ash as an enhanced settling mechanism in the water column is unlikely, as Carey (1997) observed an immediate break up of ash aggregates when impacting on the water surface. Transportation by biogenic aggregation (e.g. faecal pellets, Smayda 1971),

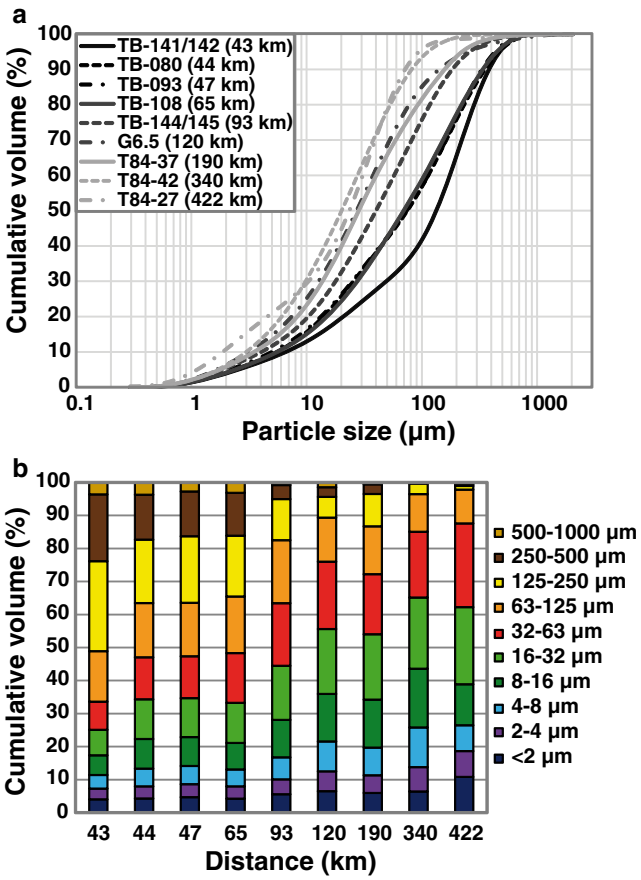

Fig. 4 (**a**) Cumulative volumes of land and sea samples (multiple samples at one station were averaged) and (**b**) cumulative volumes with distance. The coarse-size fractions decrease and the fine fraction increase with distance. The change from land to deep-sea samples lies between 93 and 120 km. There is no significant variation between the different depositional environments. Note that the two unimodal layers (26–30 cm) in T84-37 are excluded as they are likely representing the first Plinian eruption from 5 April 1815

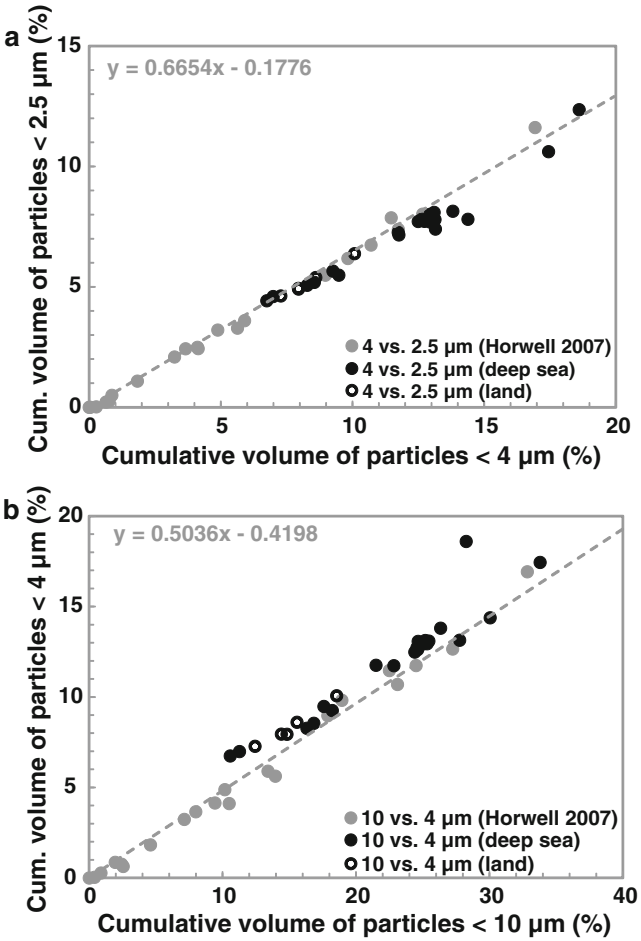

Fig. 5 Correlation plots for the volumetric proportions (**a**) 4 vs. 2.5 µm and (**b**) and 10 vs. 4 µm. *Grey circles* are size fractions from 21 volcanic eruptions of different style and distance from the vent analysed by Horwell (2007). The *black circles* show deep-sea samples, and the *white circles* represent the land samples from this study. The data suggest that even the very fine ash particles were deposited on the sea floor

on the other hand, would result in considerable deposition of organic matter within the ash layers, but detectable organic matter was not found in the studied Tambora samples. Experiments performed by Carey (1997) and Manville and Wilson (2004), as well as the observed rapid ash deposition during the Pinatubo eruption in 1991 (Wiesner et al. 2004), suggest that deposition in the deep sea occurs by vertical density currents. Vertical density currents are able to transport ash particles at least an order of magnitude faster than transport by Stokes law settling (Carey 1997), which would allow preservation of the observed grain size distribution and especially the abundance of very fine ash in the studied Tambora samples.

Bimodal and unimodal grain size distribution

The basal layer (26–30 cm depth) in core T84-37 likely represents the first Plinian event of the 1815 Tambora eruption on 5 April. During this Plinian phase, ash fall was reported in the Eastern districts of Java Island, 400 km east of the volcano (Ross 1816). Core T84-37 lies well within this distance (190 km) and direction and thus should have been within the ash fallout zone during this phase of the eruption. Further, the finer and unimodal mode compared to the overlying ash layers supports the findings of Sigurdsson and Carey (1989) that the 5 April Plinian phase was a less intense eruption (column height 33 km) than the Plinian eruption on 10 April (column height 43 km; Sigurdsson and Carey 1989).

Both cores (G6.5 and T84-37), though unimodal when averaged over their entire thickness, show a bimodal grain size distribution at 26 cm depth, which gradually changes to a unimodal and fine-grained distribution with decreasing depth.

Two main mechanisms could lead to a bimodal distribution, namely mixing of ash from the Plinian and co-ignimbrite

phase, and aggregation. We suggest that the bimodal distribution has been caused by premature fall out of airborne ash aggregates, depositing on the water surface or on land simultaneously with the coarser ash falling either as individual particles and/or being coated by finer particles. Mixing of Plinian and co-ignimbrite ash is not likely as the two phases were separated temporally by at least 3 h.

In addition, four of the five land samples (T-141/142, T-080, T-093 and T-108) show a bimodal distribution. The cause could, again, be the premature fallout of fine particles depositing at the same distance as the coarser particles.

Modelling of ash transport in the umbrella cloud

A sedimentation model was applied to the data to better understand the processes and conditions leading to the observed grain size distributions (Sparks et al. 1991; Bursik et al. 1992). The model assumes a constant source flux, radially spreading umbrella cloud in which all particle sizes are well mixed by turbulence (Sparks et al. 1991), so that the mass concentration in the umbrella cloud is given by

$$C_1 = C_0 \exp\left[-B\left(r^2 - r_0^2\right)\right] \quad (1)$$

$$B = \pi v / Q \quad (2)$$

where r (kilometres) is the radial distance from the vent, r_0 (kilometres) is the radius at the plume corner (where the plume diverts laterally), C_0 is the initial ash concentration at r_0, ν is the terminal particle settling velocity, and Q is the volumetric flow rate of the plume at the height the plume diverts laterally. The model assumes that the volumetric flow rate into the umbrella cloud, Q, remains constant. The ash depositing (per unit distance and unit width of perimeter) while the cloud advances is therefore (Sparks et al. 1991; Bursik et al. 1992)

$$C_2 = 2BrC_0 \exp\left[-B\left(r^2 - r_0^2\right)\right] \quad (3)$$

The magnitude [volume 30 km^3 DRE (Self et al. 2004) and VEI 7 (Newhall and Self 1982)] of the Tambora eruption suggests the generation of an energetic plume and umbrella cloud. The expansion velocity of large umbrella clouds in the initial stages of expansion greatly exceeds typical wind speeds (Baines and Sparks 2005), and the consequent assumption of a radially spreading gravity current without significant wind influence is in this case reasonable and is further explained below.

However, this sedimentation model is based on a gravity current with a constant flux and does not consider the fact that the cloud should decelerate markedly once an eruption stops. The remaining ash from the umbrella cloud (C_1; Eq. 1) will fall out at the end of the eruption and add to the ash deposited during the eruption (C_2; Eq. 3). It is therefore necessary to compare the total mass loading (kilograms per square metre) of both components contributing to the ash deposition. For the mass loading of the remaining ash in the umbrella cloud, the ash concentration (C_1; Eq. 1) is first multiplied by the width δr, the ring of perimeter $2\pi r$ and the cloud thickness h (considered to remain constant with distance) to get the mass in the cloud:

$$M_1 = 2\pi r \delta r h\, C_0 \exp\left[-B\left(r^2 - r_0^2\right)\right] \quad (4)$$

The mass loading is then found by dividing Eq. 4 by the area $2\pi r\delta r$:

$$m_1 = hC_0 \exp\left[-B\left(r^2 - r_0^2\right)\right] \quad (5)$$

The amount of ash depositing while the umbrella cloud spreads (C_2) is dependent on the eruption duration (T). The longer the eruption lasts, the larger the mass proportion of this component in the deposit will become. In this case, the mass flux per unit width δr and perimeter $2\pi r$ is considered (Sparks et al. 1991, and accounting for the missing B):

$$\dot{m} = 2QBC_0 r \exp\left[-B\left(r^2 - r_0^2\right)\right] \quad (6)$$

The mass loading is then found by dividing by a ring of perimeter $2\pi r$ and multiplying by time T, accounting for the eruption duration:

$$m_2 = TvC_0 \exp\left[-B\left(r^2 - r_0^2\right)\right] \quad (7)$$

Finally, the proportion of the m_1 component of the ash deposit is

$$p(m_1) = m_1/(m_1 + m_2) = h/(h + Tv) \quad (8)$$

Equation 8 shows that the proportion of ash falling out while the cloud advances (m_2) increases as the particle fall velocity (v) and/or the eruption duration (T) increase. The proportions of m_1 and m_2 are independent of distance for a given particle size, but the cumulative proportions will be distance dependent as they are the sum of all the contributions of each grain size. The proportions (Eq. 8) are then applied to the initial equations for C_1 (Eq. 1), respectively, C_2 (Eq. 3) accordingly.

The above model ignores the possibility that ash particles will be transported laterally by wind or ocean currents after leaving the base of the umbrella cloud. The role of wind is considered in "Influence of wind" section. Ocean currents could not have had a significant influence on the ash deposition, as the results demonstrate that there is no marked change in grain size distribution from land to deep-sea deposits (Fig. 4b), and even the very fine ash particles were deposited on the sea floor (Fig. 5).

Model input parameters

The Plinian phase input parameters are derived from the estimated cloud height (top of the cloud H_t) of 43 km by Sigurdsson and Carey (1989). For the co-ignimbrite phase, a cloud height (H_t) of 25 km is used, which is within the range calculated by Woods and Wohletz (1991). Table 2 lists the base height of the umbrella cloud (H_{cb}), cloud thickness (h) and radius at the plume corner (r_0) for both phases. The particle fall velocity is (Kunii and Levenspiel 1969; Bonadonna et al. 1998; Bonadonna and Phillips 2003)

$$v \approx \left(g\rho d^2 / 18\mu\right) \quad \text{for } Re < 6 \tag{9a}$$

for particles < 500 μm in this study, and

$$v \approx d\left(4\rho^2 g^2 / 225\mu\sigma\right)^{1/3} \quad \text{for } 6 \le Re < 500 \tag{9b}$$

for particles ≥ 500 μm in this study

where g is the gravitational acceleration, ρ is the particle density, d is the particle diameter, μ is the atmospheric dynamic viscosity and σ is the density of the atmosphere at the respective cloud base heights (H_{cb}; Table 2). A uniform particle density (ρ) of 2,400 kg/m^3 is assumed [dense rock equivalent of Tambora trachyandesite, 2,470 kg/m^3 (Self et al. 2004)], and for the initial relative grain concentration (C_0), the average grain size concentration over all distances is used. The particle size used for each bin is the average grain size (e.g. the 500–1,000-μm bin is represented by the 750-μm particle size, the 250–500-μm bin is represented by the 375-μm particle size, etc.).

Estimations for the volumetric flow rate (Q) into the umbrella cloud are constrained by historical accounts. Newspapers and documents published after the eruption describe in detail the 'darkness' experienced as the cloud advanced (Table 3). The velocity of the umbrella cloud is expressed by the following equation modified from Sparks (1986):

$$V = Q/(2\pi rh) \tag{10}$$

where r is the radius, and h is the plume thickness (Table 2). The model assumes that the umbrella cloud has a constant supply of mass, a constant cloud thickness and no further entrainment of air while the umbrella cloud is spreading. The onset of the Plinian eruption is documented at 7 pm 10 April. The co-ignimbrite cloud developed 3 h later, associated with pyroclastic flow formation at 10 pm 10 April. These times were used as inputs to the model.

The model results show that the historical data plot close to the volumetric flow rate profiles calculated when Q=2.2×10^{11} m^3/s for the Plinian cloud, and Q=1.5×10^{11} m^3/s for the co-ignimbrite cloud (Fig. 6 and Table 2). However, neither of the calculated profiles appears to capture an accurate timing for Bima at 60 km distance. The reported 'darkness' in Bima started at 7:00 a.m., although it is likely that the cloud reached Bima before sunrise and therefore was unnoticed by observers.

Influence of wind

The volumetric flow rate profiles of the umbrella clouds can give further information about the prevailing wind speed during the eruption. Carey and Sparks (1986) determined that the limit of an umbrella cloud crosswind spread is 1.5 times the distance to the upwind stagnation point, where the radial velocity of the cloud equals the opposing wind velocity. Tambora erupted during the onset of the easterly monsoon with little wind observed (Raffles 1835). If we assume an easterly wind, the ash sample T84-27 422 km to the north can be used as a crosswind range. With these data, the upwind range is around 280 km. The cloud velocity and therefore opposing wind speed for the umbrella cloud at this

Table 2 Input parameters for the sedimentation model

Phase	H_b (km) Neutral buoyancy height[a]	H_{cb} (km) Base height[d]	h (km) Height interval[e]	r_0 (km) Radius plume corner[f]	g (m/s^2) Gravitational acceleration[g]	μ (kg/(m s)) Dynamic viscosity[g]	σ (kg/m^3) Density[g]	Q (m^3/s) Volumetric flow rate
Plinian	30[b]	~24	~13	~7.5	9.733	1.44×10^{-5}	0.047	~2.2×10^{11}
Co-ignimbrite	~17.5[c]	~14	~7.5	~4.5	9.764	1.42×10^{-5}	0.228	~1.5×10^{11}

[a] H_b=0.7H_t (Morton et al. 1956; Bonadonna and Phillips 2003)

[b] From H=43 km (Sigurdsson and Carey 1989)

[c] H_t=25 km (23±3 km; Woods and Wohletz 1991)

[d] H_{cb}=0.8H_b (Bonadonna and Phillips 2003)

[e] h=0.3H_t (Carey and Sparks 1986)

[f] r_0~0.25H_b (Sparks et al. 1992)

[g] Standard atmosphere at base height

Table 3 Historical reports on the velocity and timing of the umbrella cloud

Location	Distance (km)	Time	Time to location (h)	Description
Bima	80	11 April, 7:00 a.m.	12[a], 9[b]	'The darkness commenced about seven in the morning.' (East India Company 1816; Ross 1816)
Makassar	380	11 April, 10:00 a.m.	15[a], 12[b]	'By ten it was so dark that I could scarcely discern the ship from the shore, though not a mile distant.' (East India Company 1816)
Banyuwangi	400	11 April, 1:00 p.m.	18[a], 15[b]	'[…] by 1 pm candles were necessary […]' (Ross 1816)
Sumenep	470	11 April, 4:00 p.m.	21[a], 18[b]	'[…] that by 4 o'clock it was necessary to light candles' (Ross 1816)
Besuki	470	11 April, 4:00 p.m.	21[a], 18[b]	'[…] we were enveloped in darkness from four o'clock P. M. of the eleventh […]' (Hubbard 1815; East India Company 1816)
Gresik	600	12 April, 8:30 a.m.	37.5[a], 34.5[b]	'[…] found it to be half past eight o'clock, I immediately went out and found a cloud of ashes descending […]' (Ross 1816)
Surakarta (Solo)	790	12 April, 4:00 p.m.	45[a], 42[b]	'At Solo, on the 12th, at 4 pm objects were not visible at 33 yards […]' (Ross 1816)

[a] Time to location after onset of eruption on 11 April 1815, 7:00 p.m. for the Plinian phase

[b] Time to location after onset of eruption on 11 April 1815, 10:00 p.m. for the co-ignimbrite phase

distance is only about 10 m/s, which does not influence greatly the circular symmetry of the umbrella cloud and ash dispersal of very high eruption columns like Tambora (Carey and Sparks 1986). Note that T84-27 at 422 km distance is the only distal crosswind sample available for this study, and the actual crosswind range could be even greater. Therefore, the calculated wind speeds could have been higher than the prevailing wind speeds during the eruption.

Sedimentation model results

Equation 8 indicates that duration (T) and fall velocity (v) are the main factors influencing the proportions of the two ash components, P_1 and P_2. In general, the majority of fine particles (low fall velocities) deposit once the eruption stops (P_1 component), while significant proportions of coarse particles (high fall velocities) fall out while the cloud advances (P_2 component). Figure 7 illustrates the relative contribution (over all distances and particle sizes) of the two ash components as a function of eruption duration. The results demonstrate that the longer the eruption lasts, the more the advancing cloud (P_2) adds to the total ash deposit. For both the Plinian and co-ignimbrite clouds, it takes less than 10 h until the P_2 component crosses the 50 % mark and consequently becomes the main component of the ash deposit (see close-up, Fig. 7). For the co-ignimbrite cloud, the P_1 component decreases a little faster than for the Plinian cloud as a consequence of the lower volumetric flow rate (Q; Fig. 6), leading to enhanced deposition. On the other hand, particles<500 μm (low Reynolds number) have higher fall velocities for the co-ignimbrite cloud as the atmospheric dynamic viscosity (μ) is slightly lower than for the Plinian cloud (Eq. 9; Table 2). The higher fall velocity leads to enhanced deposition of the fine particles during the cloud emplacement and therefore adds more of the P_2 component. The coarse ash particles (≥500 μm in this work, intermediate Reynolds number) have lower fall velocities for the co-ignimbrite cloud model with respect to the Plinian cloud due to the significantly higher air density (σ) as the

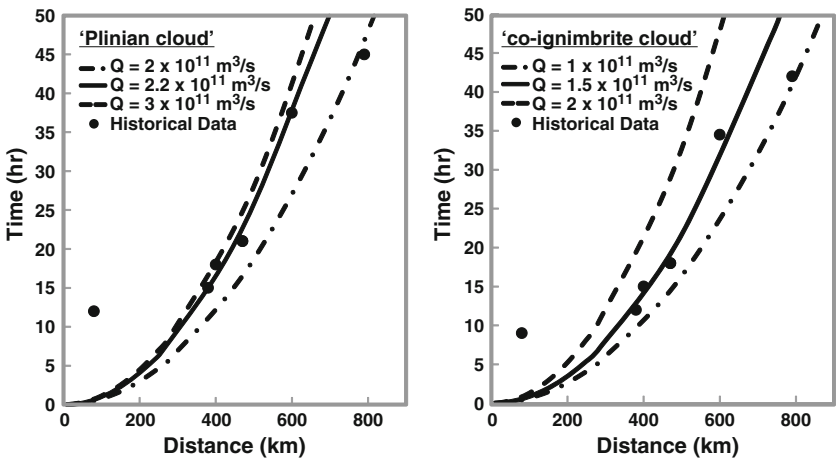

Fig. 6 Volumetric flow rate profile of the Tambora umbrella cloud for a Plinian and co-ignimbrite cloud, respectively. *Black circles* represent observed data from historical accounts (Table 2; Hubbard 1815; East India Company 1816; Ross 1816). The historical data follow very closely the profile calculated with a volumetric flow rate of $Q=2.2\times10^{11}$ m^3/s for the Plinian and $Q=1.5\times10^{11}$ m^3/s for the co-ignimbrite cloud, respectively

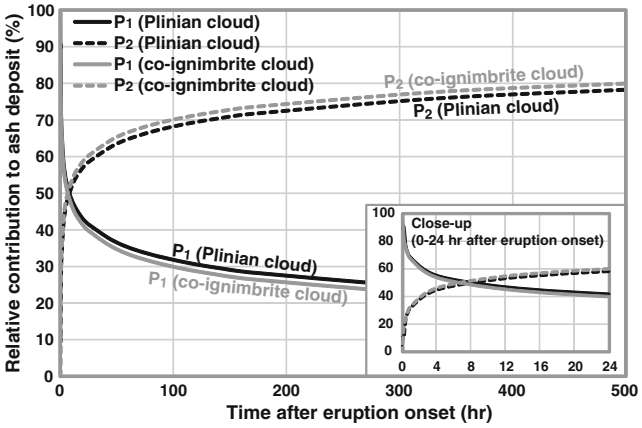

Fig. 7 Time-dependent relative contributions (in percent) of the P_1 ash component (deposition after the eruption stopped) and P_2 ash component (deposition from advancing cloud), for a Plinian and co-ignimbrite cloud (see parameters in Table 2). The longer the eruption lasts, the more ash is depositing from the advancing cloud (P_2) and the larger is the contribution to the total ash deposit

co-ignimbrite cloud is assumed to reside at a lower atmospheric level than the Plinian cloud. However, particles falling with intermediate Reynolds number (≥500 μm) are only small proportions of the deposits in the studied area, and it is therefore likely that they do not have a strong influence on the temporal evolution of the two components.

Sigurdsson and Carey (1989) argued that the bulk fall deposit (>90 km^3 tephra) of the 1815 Tambora eruption had a co-ignimbrite origin, and the duration of the preceding main Plinian phase was only about 3 h. The duration of the main eruption phase has an upper limit of 24 h, historical accounts indicate that the eruption started at about 7:00 p.m. on 10 April and continued until the evening of 11 April when continuous explosions finally ceased (Ross 1816). Using this information and the described input parameters, a mixed phase model summing a 3-h Plinian phase and a 21-h co-ignimbrite phase is simulated. Figure 8 shows the model result if considering the P_2 component only (Fig. 8a), and the result of modelling both components (P_1 and P_2) with the mixed phase scenario (3-h Plinian phase and a 21-h co-ignimbrite phase, Fig. 8b). As the P_2-only model (Fig. 8a) does not include any time constraints, the closest scenario to the mixed phase, a co-ignimbrite phase scenario, has been used for comparison. The data demonstrate that the model considering the P_2 component only fails to reproduce the observed fine ash fraction as mainly coarse ash particles deposit as the cloud advances (Fig. 8a). The observed grain size distribution can be reproduced adequately only if a finite eruption duration is considered and the ash left in the cloud at the end of the eruption is added to the deposit (Fig. 8b). The P_1 component adds more fine ash to the deposit relative to coarse ash, leading to a better agreement between the model and observed distribution. The mean deviation of the model results with respect to the observed grain size distribution is calculated by averaging the difference between model and data values at each distance for each grain size bin. The results show that the mean deviation is reduced by more than half (9.42 % to 3.73 %) if both ash components are used instead of the P_2 component only.

Even though the calculated crosswind velocity of 10 m/s likely does not have a significant influence on the ash cloud dispersal of an eruption column this high (see "Influence of wind" section), it could fractionate particles horizontally once they leave the cloud. If an average horizontal wind speed of 10 m/s is assumed, 1-mm-sized particles of the Plinian phase would deposit on the ground about 13 km (8 km for co-ignimbrite phase) from the starting position at the base of the cloud, 125 μm particles at 300 km (180 km

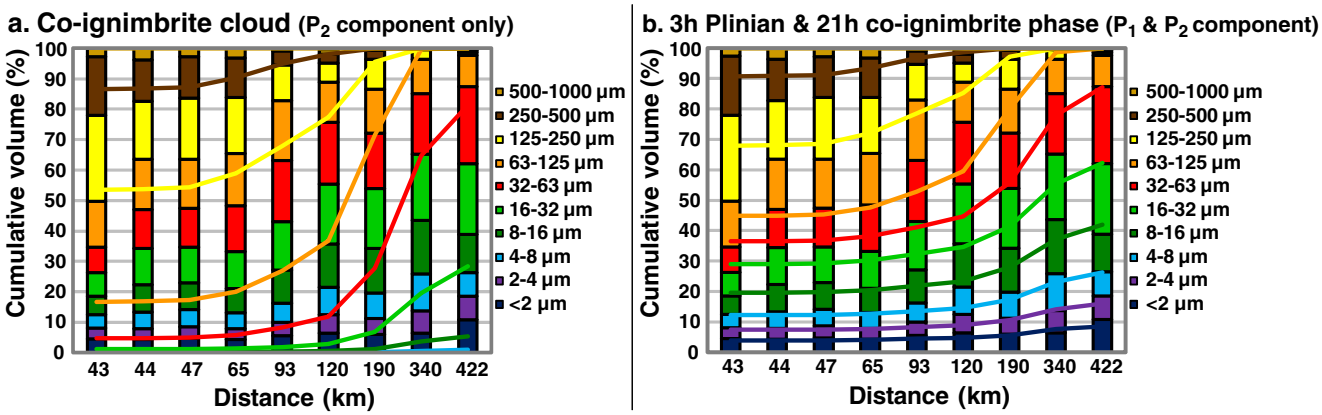

Fig. 8 Results for (**a**) a co-ignimbrite cloud modelled if the P_2 component is considered only, and (**b**) a mixed 3-h Plinian and 21-h co-ignimbrite phase modelled including the P_1 and P_2 component. The *columns* represent the observed grain size distribution, and the *solid line* represents the sedimentation model. The results show that if the ash concentration left in the cloud is added, the modelled grain size distribution has more fine ash contributing to the deposit, and gives a better fit to the observed data (decreases the model-to-data mean deviation from 9.4 % to 3.7 %). Note that the two unimodal layers (26–30 cm) in T84-37 are excluded as they likely represent the first Plinian eruption from 5 April 1815

for co-ignimbrite phase) and 16 μm particles should be carried thousands of kilometres away relative to their initial location at the base of the cloud. The fact that the model results provide a good fit to the observed data suggests that the particles leaving the base of the umbrella cloud are depositing on the ground without significant horizontal fractionation. As already recognised for numerous other eruptions (e.g. Brazier et al. 1982; Carey and Sigurdsson 1982; Scasso et al. 1994; Schumacher 1994; Brown et al. 2012), aggregation of fine particles during the sedimentation process would prevent particles from considerable fractionation. The presence of particle aggregates would further explain the grain size bimodality observed in some samples (see "Bimodal and unimodal grain size distribution" section). However, our models do not include aggregation of fine particles during the cloud emplacement, although this process is likely an important aspect of fine ash transport (e.g. Carey and Sigurdsson 1982; Durant et al. 2009). Aggregation dominantly affects very fine particles with the maximum efficiency of binding of particles due to collision being in the 40–10-μm range, based on both theory and grain size distribution of ash aggregates (e.g. Brazier et al. 1983; Gilbert and Lane 1994; Sparks et al. 1997; Brown et al. 2012). If ash aggregates are themselves small with low density, they would be dominantly retained in the cloud and therefore would not change the model significantly.

Conclusions

Grain size distributions of ash samples in the deep sea and on land have been compared and applied to an improved gravity current sedimentation model. We conclude the following:

1. The data suggest that the marine environment has not much affected the grain size characteristics of the ash fall deposit on the ocean floor and that the ash recovered from the deep sea provides continuous grain size trends with complementary land samples. Further, the volumetric proportions of the very fine grain size fraction (10 vs. 4 μm and 4 vs. 2.5 μm; Fig. 5) are similar for both depositional environments and independent of the distance from the source. The global database of marine ash is currently an underexploited resource and potentially very valuable for additional and new insights to many eruptions.
2. A rapid and effective transport mechanism, such as vertical density currents within the water column, is required to prevent size fractionation during settling in the ocean, and to maintain the similar volumetric proportions of very fine ash fraction (10 vs. 4 μm and 4 vs. 2.5 μm; Fig. 5) in the deep-sea deposits.
3. An improved atmospheric gravity current model is presented here, taking into account that once eruptions terminate the gravity current is no longer in steady-state motion. The model result is therefore a time-dependent combination of the ash depositing while the cloud advances and the remaining ash in the cloud falling out once the eruption ceases: $p=h/(h+T\nu)$. The lower the fall velocity and the shorter the eruption duration, the higher is the contribution of the ash component depositing after the eruption stops (P_1).
4. Historical accounts reporting the advancement of the umbrella cloud follow closely the volumetric flow rate profile of the umbrella cloud using $Q=2.2\times10^{11}\,m^3/s$ for a Plinian cloud, and $Q=1.5\times10^{11}\,m^3/s$ for a co-ignimbrite cloud.
5. The observed grain size distribution is in good agreement with the model result if both ash components (P_1 and P_2) are considered, using the observed maximum eruption duration of 24 h and a mixed phase eruption (3-h Plinian phase and 21-h co-ignimbrite phase). Adding the P_1 component to the model results in a better representation of the fine ash fraction, and decreases the model-to-data mean deviation from 9.4 % (if only the P_2 component is considered) to 3.73 %.
6. The bimodality observed in some ash samples, as well as the absence of substantial additional size segregation during deposition, strongly suggests that particle aggregation played a substantial role during the depositional process.

Acknowledgments This research was supported by the AXA Research Fund. We wish to thank NIOZ for providing the deep-sea cores and Charlie Mandeville for providing samples. We also acknowledge technical support and assistance from Rineke Gieles at NIOZ, as well as Rene Olsen, Danielle Cares and Rebecca Robinson at GSO Rhode Island. RSJS acknowledges a European Research Council Advanced grant. We thank Sarah Fagents, David Pyle and an anonymous reviewer for providing us with helpful and constructive comments.

References

Amante C, Eakins BW (2009) ETOPO1 1 arc-minute global relief model: procedures, data sources and analysis. National Geophysical Data Center, NOAA, Technical Memorandum NESDID NGDC-24

Baines PG, Sparks RSJ (2005) Dynamics of giant volcanic ash clouds from supervolcanic eruptions. Geophys Res Lett 32(L24808):1–2. doi:10.1029/2005GL024597

Bonadonna C, Phillips JC (2003) Sedimentation from strong volcanic plumes. J Geophys Res 108(B72340):1–2. doi:10.1029/2002JB002034

Bonadonna C, Ernst GGJ, Sparks RSJ (1998) Thickness variations and volume estimates of tephra fall deposits: the importance of particle Reynolds number. J Volcanol Geotherm Res 81:173–187. doi:10.1016/S0377-0273(98)00007-9

Brazier S, Davis AN, Sigurdsson H, Sparks RSJ (1982) Fall-out and deposition of volcanic ash during the 1979 explosive eruption of

the Soufriere of St. Vincent. J Volcanol Geotherm Res 14:335–359. doi:10.1016/0377-0273(82)90069-5
Brazier S, Sparks RSJ, Carey SN, Sigurdsson H, Westgate JA (1983) Bimodal distribution and secondary thickening in air-fall ash layers. Nature 301:115–119
Brown RJ, Bonadonna C, Durant AJ (2012) A review of volcanic ash aggregation. Phys Chem Earth A B C 45–46:65–78. doi:10.1016/j.pce.2011.11.001
Bursik MI, Sparks RSJ, Gilbert JS, Carey SN (1992) Sedimentation of tephra by volcanic plumes: I. Theory and its comparison with a study of the Fogo A Plinian deposit, Sao Miguel (Azores). Bull Volcanol 54(4):329–344. doi:10.1007/BF00301486
Carey SN (1997) Influence of convective sedimentation on the formation of widespread tephra fall layers in the deep sea. Geology 25(9):839–842. doi:10.1130/0091-7613(1997)025<0839:IOCSOT>2.3.CO;2
Carey SN, Sigurdsson H (1982) Influence of particle aggregation on deposition of distal tephra from the May 18, 1980, eruption of Mount St. Helens volcano. J Geophys Res 87(B8):7061–7072. doi:10.1029/JB087iB08p07061
Carey SN, Sparks RSJ (1986) Quantitative models of the fallout and dispersal of tephra from volcanic eruption columns. Bull Volcanol 48(2–3):109–125. doi:10.1007/BF01046546
Casadevall TJ (1994) The 1989–1990 eruption of Redoubt volcano, Alaska: impacts on aircraft operations. J Volcanol Geotherm Res 62(1–4):301–316. doi:10.1016/0377-0273(94)90038-8
Crawfurd J (1856) A descriptive dictionary of the Indian islands and adjacent countries. Bradbury and Evans, London
Durant AJ, Rose WI, Sarna-Wojcicki AM, Carey SN, Volentik ACM (2009) Hydrometeor-enhanced tephra sedimentation: constraints from the 18 May 1980 eruption of Mount St. Helens. J Geophys Res 114:B03204
East India Company (1816) The Asiatic journal and monthly miscellany, vol 2. Allen & Co, London
ESRI (2009) World shaded relief. http://services.arcgisonline.com/ArcGIS/rest/services/World_Shaded_Relief/MapServer. Accessed 6 September 2010
Fisher RV (1965) Settling velocity of glass shards. Deep-Sea Res 12:345–353. doi:10.1016/0011-7471(65)90006-9
Gilbert JS, Lane SJ (1994) The origin of accretionary lapilli. Bull Volcanol 56:398–411
Horwell CJ (2007) Grain-size analysis of volcanic ash for the rapid assessment of respiratory health hazard. J Environ Monit 9:1107–1115. doi:10.1039/b710583p
Hubbard AH (1815) Java Government Gazette No.169, May 20, 1815. Hubbard AH, Batavia
Kunii D, Levenspiel O (1969) Fluidization engineering. Wiley, New York
Manville V, Wilson CJN (2004) Vertical density currents: a review of their potential role in the deposition and interpretation of deep-sea ash layers. J Geol Soc Lond 161:947–958. doi:10.1144/0016-764903-067
Morton BR, Taylor G, Turner JS (1956) Turbulent gravitational convection from maintained and instantaneous sources. Proc Roy Soc Lond A 234:1–23. doi:10.1098/rspa.1956.0011
Newhall CG, Self S (1982) The volcanic explosivity index (VEI): an estimate of explosive magnitude for historical volcanism. J Geophys Res 87(C2):1231–1238. doi:10.1029/JC087iC02p01231
Raffles TS (1817) The history of Java. Black, Parbury and Allen, London
Raffles S (1835) Memoir of the life and public services of Sir Thomas Stamford Raffles. James Duncan, London
Rose WI, Chesner CA (1987) Dispersal of ash in the great Toba eruption, 75 ka. Geology 15(10):913–917. doi:10.1130/0091-7613(1987)15<913:DOAITG>2.0.CO;2
Rose WI, Durant AJ (2009) Fine ash content of explosive eruptions. J Volcanol Geotherm Res 186(1–2):32–39. doi:10.1016/j.jvolgeores.2009.01.010
Ross JT (1816) Narrative of the effects of the eruption from the Tomboro Mountain, in the island of Sumbawa, on the 11th and 12th April 1815. In: Verhandelingen van het Bataviaasch Genootschap, der Kunsten en Wetenschappen. Hubbard, Batavia
Scasso RA, Corbella H, Tiberi P (1994) Sedimentological analysis of the tephra from the 12–15 August 1991 eruption of Hudson volcano. Bull Volcanol 56:121–132. doi:10.1007/BF00304107
Schumacher R (1994) A reappraisal of Mount St. Helens' ash clusters—depositional model from experimental observation. J Volcanol Geotherm Res 59(3):253–260. doi:10.1016/0377-0273(94)90099-X
Self S, Gertisser R, Thordarson T, Rampino MR, Wolff JA (2004) Magma volume, volatile emissions, and stratospheric aerosols from the 1815 eruption of Tambora. Geophys Res Lett 31(L20608). doi:10.1029/2004GL020925
Sigurdsson H, Carey SN (1989) Plinian and co-ignimbrite tephra fall from the 1815 eruption of Tambora volcano. Bull Volcanol 51(4):243–270. doi:10.1007/BF01073515
Sigurdsson H, Sparks RSJ, Carey SN, Huang TC (1980) Volcanogenic sedimentation in the Lesser Antilles Arc. J Geol 88(5):523–540
Smayda TJ (1971) Normal and accelerated sinking of phytoplankton in the sea. Mar Geol 11:105–122. doi:10.1016/0025-3227(71)90070-3
Sparks RSJ (1986) The dimensions and dynamics of volcanic eruption columns. Bull Volcanol 48(1):3–15. doi:10.1007/BF01073509
Sparks RSJ, Carey SN, Sigurdsson H (1991) Sedimentation from gravity currents generated by turbulent plumes. Sedimentology 38(5):839–856. doi:10.1111/j.1365-3091.1991.tb01875.x
Sparks RSJ, Bursik MI, Ablay GJ, Thomas RME, Carey SN (1992) Sedimentation of tephra by volcanic plumes. Part 2: controls on thickness and grain-size variations of tephra fall deposits. Bull Volcanol 54(8):685–695. doi:10.1007/BF00430779
Sparks RSJ, Bursik MI, Carey SN, Gilbert JS, Glaze LS, Sigurdsson H, Woods AW (1997) Volcanic plumes. Wiley, London
Stewart GA (1820) Description of a volcanic eruption in the island of Sumbawa. Trans Lit Soc Bombay 2:109–114
Stothers RB (1984) The great Tambora eruption in 1815 and its aftermath. Science 224:1191–1198. doi:10.1126/science.224.4654.1191
Watkins ND, Sparks RSJ, Sigurdsson H, Huang TC, Federman A, Carey SN, Ninkovich D (1978) Volume and extent of the Minoan tephra from Santorini volcano: new evidence from deep-sea sediment cores. Nature 271:122–126. doi:10.1038/271122a0
Wiesner MG, Wetzel A, Catane SG, Listanco EL, Mirabueno HT (2004) Grain size, areal thickness distribution and controls on sedimentation of the 1991 Mount Pinatubo tephra layer in the South China Sea. Bull Volcanol 66(3):226–242. doi:10.1007/s00445-003-0306-x
Woods AW, Wohletz K (1991) Dimensions and dynamics of co-ignimbrite eruption columns. Nature 350:225–227. doi:10.1038/350225a0
Zen M, Ganie B (1992) Tambora 1815 eruption. In: Degens ET, Wong HK, Zen MT (eds) The sea off Mount Tambora. Mitteilungen aus dem Geologisch-Paläontologischen Institut der Universität Hamburg Heft 70, Hamburg, pp 173–185
Zollinger H (1855) Besteigung des Vulkanes Tambora auf der Insel Sumbawa und Schilderung der Erupzion desselben im Jahr 1815. J. Wurster and Co, Winterthur